21st Australasian Fluid Mechanics Conference
Adelaide, Australia
10-13 December 2018

A study of inertial particle focusing in curved microfluidic ducts with large bend radius and low flow rate

Brendan Harding

School Of Mathematical Sciences, The University of Adelaide
Adelaide, South Australia 5005, Australia

Abstract

Inertial lift is a fluid phenomena exploited in microfluidic devices to separate particles/cells based on their size. Whilst it has been studied extensively for spherical particles suspended in flow through straight ducts, typically of rectangular shape, many applications involve ducts that are curved. This paper explores the estimation of focusing behaviour in curved ducts by simply adding inertial lift forces computed for a straight duct (having the same cross-section) to the drag forces within the cross-sectional plane which are generated by the secondary motion of the fluid flow through the curved duct. We examine the specific case of a curved rectangular duct with height ℓ, width 2ℓ and bend radius R in which a neutrally buoyant particle with radius a is suspended. The simple force model is appropriate when R is large and the flow rate is low such that the Dean number is small. The magnitude of the secondary flow drag relative to the inertial lift force scales with $\kappa = \ell^4/(a^3R)$ and the dominant focusing behaviour is found to approximately collapse onto a single curve when plotted against κ, particularly when $\kappa \leq 30$.

Introduction

In this study the perturbing force on a neutrally buoyant particle suspended in flow through a curved duct having a rectangular cross-section is approximated by adding the lift force experienced by the particle in a straight duct to the drag force from the secondary motion of a fluid flowing through a curved duct (having the same cross-section in each case). This approximation was suggested in the microfluidics literature [2] but has yet to have been investigated in detail to the best of our knowledge. Whilst it has also been suggested that the modification of the axial flow profile at higher Dean numbers may also play a role [8] we restrict this study to small Dean numbers. Experiments typically involve spiral shape devices although it has been observed that the flow in a spiral is close to that obtained by treating the bend radius to be (locally) constant [4]. As such we expect that studies of inertial lift in ducts having constant bend radius will provide a good estimate of the focusing behaviour in a spiral device having similar bend radius near the outlet.

We begin by briefly outlining the way in which both the inertial lift force and the drag force from the secondary fluid motion are estimated. The calculation of the inertial lift force assumes that the particle Reynolds number Re_p is small and is based upon the approach in [5]. In particular, the inertial lift is calculated for a particle suspended in Poiseuille flow through a straight duct. This is sensible if one assumes that the bend radius is sufficiently large that any local of portion of the duct around a particle can be reasonably approximated as straight and, additionally, the Dean number Dn is small enough that the main axial flow in the corresponding curved duct is close to Poiseuille flow. Given that Dn is taken to be small we approximate the steady fluid flow through a curved duct (in the absence of a particle) using a perturbation expansion with respect to $K = \mathrm{Dn}^2$ which leads to a convenient separation of the leading order components of the axial and secondary flow motion. The drag force from the secondary flow motion can then be approximated by solving an appropriate Stokes problem in the straight duct whereby the secondary flow velocity is used to impose boundary conditions on the particle. The inertial lift and drag forces are then combined and it is observed that the scale of the secondary flow drag relative to the inertial lift force is given by $\kappa = \ell^4/a^3R$.

The combined force is then examined for four different particle sizes. With a fixed bend radius we observe a vertically symmetric pair of stable equilibria within the cross-section towards which the majority of particles will eventually migrate/focus. The horizontal location of the pair differs for each particle size due to the way the inertial lift force and secondary flow drag interact. Upon examining how the horizontal location varies with the bend radius it is found that the ordering of focused particles changes several times in relation to their size. This behaviour is observed to approximately collapse onto a single curve when plotted against κ, particularly for smaller values of κ. For $\kappa \ll 30$ and $\kappa \gg 30$ the majority of particles migrate towards the centre (horizontally), whilst in between particles migrate towards the inside wall. We conclude that the dimensionless parameter κ could potentially be useful in characterising the focusing behaviour of particles within curved ducts under appropriate flow conditions and that this warrants further investigation.

Methodology

Estimation of the inertial lift force

The inertial lift force on a neutrally buoyant spherical particle with radius a suspended in flow through a straight duct is estimated via the perturbation expansion of the inertial lift force developed in [5, 6]. Let μ, ρ denote the viscosity and density of the fluid respectively. Consider a straight duct with rectangular cross-section $[-\ell,\ell]\times[-\ell/2,\ell/2]$ (i.e. having width 2ℓ and height ℓ) through which there is a steady pressure driven flow in the z direction with velocity distribution $\bar{\boldsymbol{u}}_s = (0,0,\bar{w}_s)$. We refer to $\bar{\boldsymbol{u}}_s$ as the background flow which in this case is simply Poiseuille flow through the duct (the subscript s is used to differentiate this from steady flow in a curved duct introduced later). Now consider adding the particle to the flow and suppose at some moment in time it is located at $\boldsymbol{x}_p = (x_p, y_p, 0)$ with $x_p \in [-\ell+a, \ell-a]$ and $y_p \in [-\ell/2+a, \ell/2-a]$ and has (constant) velocity $\boldsymbol{u}_p = (0,0,w_p)$ and spin $\boldsymbol{\Omega}_p = (\Omega_{p,x}, \Omega_{p,y}, 0)$. The estimation of the inertial lift force L_x, L_y in the x, y directions respectively acting on the particle at this instant are then estimated as follows. One first determines the leading order disturbance to the background flow, denoted as the disturbance pressure q_0 and velocity $\boldsymbol{v}_0$, which is the solution to

$$-\nabla q_0 + \mu\nabla^2\boldsymbol{v}_0 = \boldsymbol{0}, \qquad \nabla\cdot\boldsymbol{v}_0 = 0, \tag{1}$$

with the boundary conditions $\boldsymbol{v}_0 = \boldsymbol{0}$ on the duct walls and $\boldsymbol{v}_0 = \boldsymbol{\Omega}_p \times (\boldsymbol{x}-\boldsymbol{x}_p) + \boldsymbol{u}_p - \bar{\boldsymbol{u}}_s$ on the particle surface. In solving this equation one determines the values of $w_p, \Omega_{p,x}, \Omega_{p,y}$ such that the there is no net force or torque on the particle from the $q_0, \boldsymbol{v}_0$

component of the disturbance flow, that is

$$\mathbf{0} = \int_{|\boldsymbol{x}-\boldsymbol{x}_p|=a} -q_0\boldsymbol{n} + \mu\boldsymbol{n}\cdot\left(\nabla\boldsymbol{v}_0 + \nabla\boldsymbol{v}_0^{\mathsf{T}}\right) dS, \tag{2}$$

$$\mathbf{0} = \int_{|\boldsymbol{x}-\boldsymbol{x}_p|=a} (\boldsymbol{x}-\boldsymbol{x}_p)\times\left(-q_0\boldsymbol{n} + \mu\boldsymbol{n}\cdot\left(\nabla\boldsymbol{v}_0 + \nabla\boldsymbol{v}_0^{\mathsf{T}}\right)\right) dS, \tag{3}$$

where the normal $\boldsymbol{n}$ is taken as pointing outwards from the particle centre. Note it is sufficient to consider only the z component of (2) and the x,y components of (3). The inertial lift force L_x, L_y can then be estimated from forces on the particle exerted by the next order approximation of the disturbance flow with respect to the particle Reynolds number $\mathrm{Re}_p = (\rho/\mu)U_m a^2/\ell$ (where U_m is the maximum of $\bar{\boldsymbol{u}}_s$). However, a form of the Lorentz reciprocal theorem allows L_x, L_y to be estimated directly from $q_0, \boldsymbol{v}_0$ as

$$L_* := -\rho\int_{\mathcal{F}} \hat{\boldsymbol{u}}_*\cdot\left(\boldsymbol{v}_0\cdot\nabla\bar{\boldsymbol{u}}_s + (\boldsymbol{v}_0 + \bar{\boldsymbol{u}}_s - \boldsymbol{u}_p)\cdot\nabla\boldsymbol{v}_0\right) dV,$$

for $* = x, y$, where $\mathcal{F}$ denotes the fluid domain (i.e. the interior of the duct excluding the particle) and the velocity term $\hat{\boldsymbol{u}}_*$, along with a pressure $\hat{p}_*$, solve (1) with the boundary condition $\hat{\boldsymbol{u}}_* = \mathbf{0}$ on the duct walls and $\hat{\boldsymbol{u}}_* = \hat{\boldsymbol{e}}_*$ on the particle surface (with $\hat{\boldsymbol{e}}_*$ denoting the usual unit normal in the $*$ direction).

This brief account has been given in a dimensional setting but is straightforward to non-dimensionalise via the spatial scale a and velocity scale $U_m a/\ell$ (with remaining quantities then following the standard non-dimensionalisation of viscous flows, see [5]). Note in particular that this leads to a non-dimensionalisation of the lift force as $(L_x, L_y) = (\rho U_m^2 a^4/\ell^2)(\hat{L}_x, \hat{L}_y)$. The resulting $(\hat{L}_x, \hat{L}_y)$ is strongly dependent on the particle position (x_p, y_p) whereas changes with respect to a/ℓ are generally subtle.

We estimate $\hat{L}_x, \hat{L}_y$ by solving the requisite Stokes problems using the finite element method. The computational domain consists of a portion of the (straight) duct in a neighbourhood of the particle discretised with upwards of 10^6 tetrahedral cells. The solution of the standard weak form of (1) using a Taylor–Hood (P_2, P_1) basis is implemented using the FEniCS framework [7, 1]. The inertial lift force is calculated with the particle centred at a large number of equally spaced points within the cross-section which are then interpolated using a bivariate spline of degree 3. To avoid difficulties that can arise when the particle surface is very close to a wall we only compute $\hat{L}_x, \hat{L}_y$ for particles placed at least $\ell/40$ away from the duct walls.

Estimation of drag force from secondary flow motion

To estimate the drag forces on the particle from the secondary fluid motion within the curved duct we first approximate the steady fluid flow using the Rayleigh–Ritz approximation described in [3]. The method is derived via a perturbation expansion of the background flow with respect to the square of the Dean number $K = \mathrm{Dn}^2$ where $\mathrm{Dn} = (\rho/\mu)U_m(\ell/2)\sqrt{\delta}$ and $\delta = \ell/2R$. This allows the flow to be expanded as

$$\bar{w}(x,y) = \sum_{n=0}^{\infty} K^n \bar{w}_n(x,y), \qquad \Phi(x,y) = \sum_{n=0}^{\infty} K^n \Phi_n(x,y),$$

where $\bar{w}$ denotes the axial flow velocity and Φ denotes the stream-function of the secondary flow. A (bivariate) polynomial approximation to each $\bar{w}_n, \Phi_n$, up to some finite N, is obtained by finding the coefficients that minimise appropriate functionals. The separation of the axial and secondary flow components proportional to powers of K is particularly useful in this context where we require only an approximation of the secondary flow drag up to the same power of U_m to which the inertial lift force is estimated. This would be more difficult with an expansion of the background flow with respect to δ which is another common choice in studies of flow through curved ducts, see for example [9]. Another advantage of the method is that it handles different cross-section shapes with ease which, although not needed for this particular study, is anticipated to be useful in future studies involving non-rectangular cross-sections.

For small Dn we note that it is sufficient to approximate the flow via the leading order terms $\bar{w}_0, \Phi_0$. Furthermore, given large R, one may also use the Dean approximation in which case one has

$$-\frac{G}{\mu} = \frac{\partial^2\bar{w}_0}{\partial x^2} + \frac{\partial^2\bar{w}_0}{\partial y^2},$$

$$\frac{\rho}{\mu}\frac{2\bar{w}_0}{R}\frac{\partial\bar{w}_0}{\partial y} = \frac{\partial^4\Phi_0}{\partial x^4} + 2\frac{\partial^4\Phi_0}{\partial x^2\partial y^2} + \frac{\partial^4\Phi_0}{\partial y^4},$$

along with no-slip boundary conditions, where G is a pressure gradient driving the flow. The resulting approximation of the axial flow component $\bar{w} \approx \bar{w}_0$ is exactly Poiseuille flow through a straight duct further justifies why the inertial lift force in the curved duct can be estimated using a straight duct. The leading order x,y components of the fluid velocity, denoted $\bar{u}_0, \bar{v}_0$ respectively, are recovered via $\partial\Phi_0/\partial x = \bar{v}_0$ and $\partial\Phi_0/\partial y = -\bar{u}_0$. With $U_m = \max\bar{w}_0$ then $\bar{u}_0, \bar{v}_0$ can be shown to scale as $\mathrm{Dn}\sqrt{\delta}U_m$ and thus we introduce the dimensionless variables $(\bar{u}_0, \bar{v}_0) = \sqrt{\delta}\,\mathrm{Dn}\,U_m(\hat{\bar{u}}_0, \hat{\bar{v}}_0)$ such that the resulting $\hat{\bar{u}}_0, \hat{\bar{v}}_0$ are effectively independent of R.

Given $\bar{u}_0, \bar{v}_0$, the resulting drag on a small spherical particle (with radius a and centred at $\boldsymbol{x}_p$) could be estimated via Stokes drag law. However, the resulting estimate fails to take into account the effect of the finite size of the particle and the duct walls. A better approximation of the drag force from the secondary fluid motion, denoted D_x, D_y, can be obtained by solving an additional Stokes problem in the straight duct and integrating the resulting fluid stresses over the particle surface. One first finds $\boldsymbol{v}_c, q_c$ which solve (1) with the boundary condition $\boldsymbol{v}_c = \mathbf{0}$ on the walls of the duct and $\boldsymbol{v}_c = -\bar{u}_0\hat{\boldsymbol{e}}_x - \bar{v}_0\hat{\boldsymbol{e}}_y$. Each D_x, D_y is then estimated via

$$D_* = \hat{\boldsymbol{e}}_*\cdot\int_{|\boldsymbol{x}-\boldsymbol{x}_p|=a} -q_c\boldsymbol{n} + \mu\boldsymbol{n}\cdot\left(\nabla\boldsymbol{v}_c + \nabla\boldsymbol{v}_c^{\mathsf{T}}\right) dS.$$

We again use the finite element method for these calculations. The drag can be non-dimensionalised as $(D_x, D_y) = \mu a\sqrt{\delta}\,\mathrm{Dn}\,U_m(\hat{D}_x, \hat{D}_y)$. The resulting $(\hat{D}_x, \hat{D}_y)$ is strongly dependent on the particle location (x_p, y_p) whereas changes with respect to a/ℓ are relatively small. Note that z component of the drag is neglected since the particle was assumed to have reached terminal velocity in this direction for the purpose of estimating the inertial lift force.

Combining the two forces

Given the first order estimates of L_x, L_y and D_x, D_y we now need only add the two and analyse the resulting force to determine if there exist equilibrium positions within the duct cross-section which particles will migrate towards. In dimensional form one obtains

$$F_* := L_* + D_* = \rho U_m^2\frac{a^4}{\ell^2}\hat{L}_*(x_p, y_p) + \frac{1}{4}\rho U_m^2\frac{a\ell^2}{R}\hat{D}_*(x_p, y_p),$$

for each $* = x, y$. It is convenient to non-dimensionalise the total force via the scaling of the inertial lift component, that is upon setting $(F_x, F_y) = (\rho U_m^2 a^4/\ell^2)(\hat{F}_x, \hat{F}_y)$ one obtains

$$\hat{F}_*(x_p, y_p) = \hat{L}_*(x_p, y_p) + \frac{\kappa}{4}\hat{D}_*(x_p, y_p), \tag{4}$$

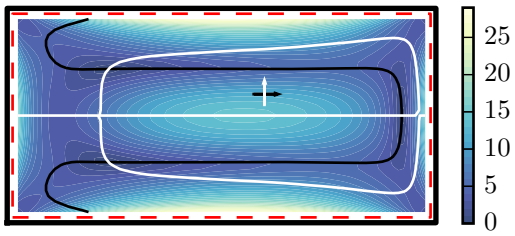

Figure 1: Magnitude of the total force $(\hat{F}_x, \hat{F}_y)$ on a particle with radius $2a/\ell = 0.05$. See text for a description.

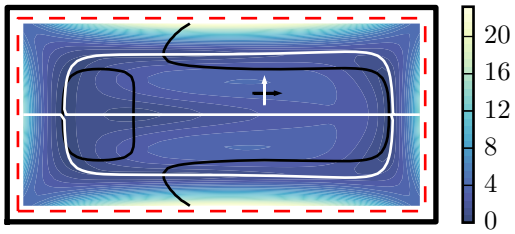

Figure 2: Magnitude of the total force $(\hat{F}_x, \hat{F}_y)$ on a particle with radius $2a/\ell = 0.10$. See text for a description.

where $\kappa := \ell^4/a^3R$ captures the magnitude of the secondary flow drag relative to the inertial lift force. The location of equilibria within the cross-section for a given particle size are the zeros of $(\hat{F}_x(x_p, y_p), \hat{F}_y(x_p, y_p))$ and the stability of each is straightforward to determine from the eigenvalues of the Jacobian.

Results and discussion

We examine the total force (4) for four different sized particles, specifically $2a/\ell = 0.05, 0.10, 0.15, 0.20$. In Figures 1,2,3,4 we plot the magnitude of the force on the particle (that is $(\hat{F}_x^2 + \hat{F}_y^2)^{0.5}$) for each particle size and with $\delta = 0.001$. To aid in the identification of equilibria we also plot the zero level set contour of $\hat{F}_x$ (black) and $\hat{F}_y$ (white). Equilibrium positions are located where the two zero level set contours intersect. Arrows indicate the sign of $\hat{F}_x$ (black) and $\hat{F}_y$ (white) in one particular region. These can be used to visually identify the stability of some equilibria noting that the sign changes whenever the corresponding zero contour line is crossed.

In Figure 1, where $2a/\ell = 0.05$, the inertial lift force and secondary drag have similar magnitude and interact to produce the total force shown. Three equilibria are readily identified, one near the right (outside) wall of the duct which is unstable, and a pair near the left (inside) wall of the duct which are positioned symmetrically with respect to y. The stability of the latter two is difficult to infer visually in this case but the eigenvalues of the Jacobian are negative and thus they are stable. Further examination suggests that all particles initially in the upper half will migrate to the upper of the stable equilibria pair whilst those initially in the lower half will migrate towards the lower of the equilibria pair.

In Figures 2,3,4, where $2a/\ell = 0.10, 0.15, 0.20$ respectively, the secondary flow drag is becoming smaller relative to the inertial lift force as the particle size increases. Five equilibria are readily identified in the latter two figures whereas there are seven in Figure 2 (three are near the left wall where the zero contour lines of $\hat{F}_x, \hat{F}_y$ are almost overlapping and are difficult to identify visually). In Figures 3 and 4 the three equilibria centred vertically are unstable whilst the remaining symmetric pair is stable.

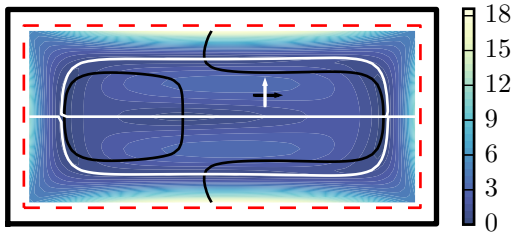

Figure 3: Magnitude of the total force $(\hat{F}_x, \hat{F}_y)$ on a particle with radius $2a/\ell = 0.15$. See text for a description.

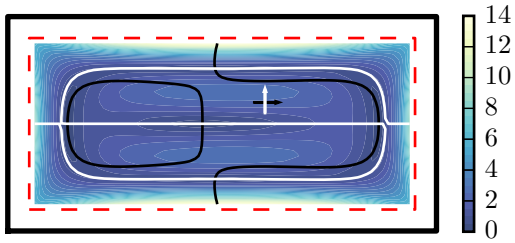

Figure 4: Magnitude of the total force $(\hat{F}_x, \hat{F}_y)$ on a particle with radius $2a/\ell = 0.20$. See text for a description.

All particles will again migrate towards one of the two stable equilibria depending on whether they are initially in the upper of lower half. Three of the seven equilibria in Figure 2 are stable, two are again the symmetric pair whilst a third is close to the left wall and centred vertically. The additional stable equilibria near the left wall is effectively a left over equilibria that occurs for small particles travelling through straight rectangular ducts for which it is known relatively few particles will migrate towards [6]. Observe there are three unstable equilibria in close proximity which effectively repel particles from this additional stable equilibria that are not sufficiently close to it initially.

The horizontal location of the stable equilibrium pair that occurs in each case shifts from being near the left (inside) wall towards the centre for increasing particle size. This is suggestive of the size based focusing that is observed and exploited in spiral microfluidic devices. To examine how this is influenced by the bend radius we plot the horizontal location of the stable equilibria for each particle size over a range of δ^{-1} (or equivalently R) in Figure 5. The main effect of changing δ^{-1} is a change in a magnitude of the secondary drag relative to the inertial lift force. There are several things to note in this plot. The first is that for very large $2R/\ell$ a stable equilibria appears near the right wall for the smallest particle (at around $2R/\ell = 8192$). Likewise, additional stable equilibria appear near the left wall for the two smaller particle sizes, although they first appear for smaller $2R/\ell$ (at around $2R/\ell = 724, 4096$ for $2a/\ell = 0.10, 0.05$ respectively). These are explained by the secondary flow drag vanishing for large δ^{-1} leaving only the inertial lift force which predicts the extra equilibria near the side walls of a straight rectangular duct for sufficiently small particles. As noted previously, relatively few particles are expected to migrate towards these additional equilibria in practice and so these points will be ignored in the remainder of the discussion. The remaining points in the plot correspond to the horizontal location of the vertically symmetric stable equilibria pair. Observe the behaviour is somewhat complex with the ordering of the focusing position with respect to the different particle sizes changing several times over the range of $2R/\ell$ considered. For example, at $\delta^{-1} = 30$ the ordering of the particles is largest to smallest going from the inside wall towards the centre of the

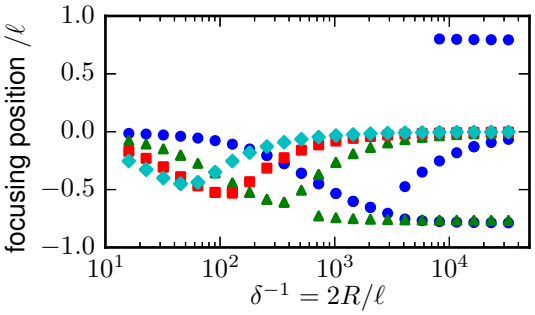

Figure 5: Focusing position of different size particles versus $\delta^{-1} = 2R/\ell$. Particle sizes (expressed as $2a/l$) are 0.05 (blue, circle), 0.10 (green, triangle), 0.15 (red, square) and 0.20 (cyan, diamond).

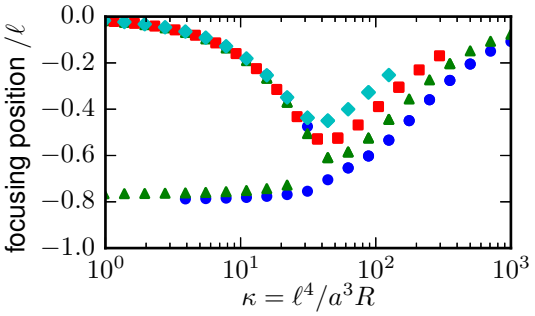

Figure 6: Focusing position of different size particles versus ℓ^4/a^3R. Particle labels are the same as in Figure 5. Note that the data for different size particles covers different portions of the range of the horizontal axis. Also note that the vertical axis includes only the half of the duct toward the inside of the bend.

duct. On the other hand, at $\delta^{-1} = 1000$ the ordering is reversed (ignoring the additional equilibria of the second smallest particle). Numerous other orderings can be observed for values of δ^{-1} in between these two examples. These results suggest that the order in which different sized particles are collected in a spiral microfluidic device may be quite sensitive to the bend radius near the outlet.

In Figure 6 we plot the same data but this time against the ratio $\kappa = \ell^4/a^3R$. Here we observe that the curves approximately collapse, especially so in the half with $\kappa < 30$. Small values of κ are where the inertial lift force is dominant whilst large values are where the secondary flow drag is dominant. Note the additional 'tail' near the left wall for the two smaller particle sizes with $\kappa < 30$ is again the additional equilibria near the left wall in which relatively few particles are expected to be found in practice. For the remaining points we observe the general trend is for particles to focus near the centre for small κ, and migrate towards the left (inside) wall as κ increases and then back towards the centre for very large κ. Another trend highlighted in this figure is that smaller particles get much closer to the inside wall than larger particles before migrating back towards the centre. Recall that this model of the total force is generally only expected to be valid when R is quite large (and thus for small κ). Nonetheless the extrapolated results for larger κ provide some insight into what might occur for smaller values of R. Interestingly our results never predict the horizontal location of the dominant equilibria pair to be on the right side of the duct whereas some experimental results do predict particles in this region [8]. This behaviour may be an effect of higher flow rates, e.g. in which the background flow profile becomes increasingly skewed towards the outer wall, which is not captured by this simple model.

Conclusions

We have investigated a simple model for estimating the focusing behaviour of particles in curved ducts by superimposing the inertial lift force in a straight duct with the drag force from the secondary component of the Dean flow that develops in curved ducts as suggested in [2]. Our brief investigation for a duct having a rectangular cross-section demonstrates that the focusing order is quite sensitive to both the particle size and bend radius. Further, whilst this behaviour initially seems quite complex we show that it approximately collapses onto a single curve when plotted against the ratio $\kappa = \ell^4/a^3R$. The dominant stable equilibria pair, which originates from inertial lift forces in a straight duct, is found to shift towards the inside wall and then back towards the centre with increasing κ. The dimensionless parameter κ could potentially be applied to estimate the focusing position of particles through curved rectangular microfluidic ducts operating at a sufficiently low flow rate. This brief study could be extended in several ways including (but not limited to) an investigation of additional cross-section shapes, further comparison with experimental data and development of a more general model.

Acknowledgements

This research was supported under Australian Research Council's Discovery Projects funding scheme (project number DP160102021). Some of the results were calculated using supercomputing resources provided by the Phoenix HPC service at the University of Adelaide.

References

[1] Alnæs, M., Blechta, J., Hake, J., Johansson, A., Kehlet, B., Logg, A., Richardson, C., Ring, J., Rognes, M. and Wells, G., The FEniCS project version 1.5, *Archive of Numerical Software*, **3**.

[2] Di Carlo, D., Inertial microfluidics, *Lab Chip*, **9**, 2009, 3038–3046.

[3] Harding, B., A rayleigh–ritz method for navier–stokes flow through curved ducts, *ANZIAMJ*, accepted.

[4] Harding, B. and Stokes, Y., Fluid flow in a spiral microfluidic duct, *Physics of Fluids*, **30**, 2018, 042007.

[5] Hood, K., Lee, S. and Roper, M., Inertial migration of a rigid sphere in three-dimensional poiseuille flow, *Journal of Fluid Mechanics*, **765**, 2015, 452479.

[6] Hood, K. T., *Theory of Particle Focusing in Inertial Microfluidic Devices*, Ph.D. thesis, University of California, Los Angeles, 2016.

[7] Logg, A., Mardal, K.-A. and Wells, G. N., *Automated Solution of Differential Equations by the Finite Element Method*, Springer, 2012.

[8] Martel, J. M. and Toner, M., Particle focusing in curved microfluidic channels, *Scientific Reports*, **3**.

[9] Yanase, S., Kaga, Y. and Daikai, R., Laminar flows through a curved rectangular duct over a wide range of the aspect ratio, *Fluid Dynamics Research*, **31**, 2002, 151.